Published in final edited form as:
ACS Nano. 2020 June 23; 14(6): 7181–7190. doi:10.1021/acsnano.0c02138.

Coassembly-Induced Transformation of Dipeptide Amyloid-Like Structures into Stimuli-Responsive Supramolecular Materials

Wei Ji,
Department of Molecular Microbiology and Biotechnology, George S. Wise Faculty of Life Sciences, Tel Aviv University, Tel Aviv 6997801, Israel

Chengqian Yuan
State Key Laboratory of Biochemical Engineering, Institute of Process Engineering, Chinese Academy of Sciences, 100190 Beijing, China

Priyadarshi Chakraborty,
Pandeeswar Makam,
Santu Bera,
Sigal Rencus-Lazar
Department of Molecular Microbiology and Biotechnology, George S. Wise Faculty of Life Sciences, Tel Aviv University, Tel Aviv 6997801, Israel

Junbai Li*,
Beijing National Laboratory for Molecular Sciences, CAS Key Lab of Colloid Interface and Chemical Thermodynamics, Institute of Chemistry, Chinese Academy of Sciences, Beijing 100190, China

Xuehai Yan*,
State Key Laboratory of Biochemical Engineering, Institute of Process Engineering, Chinese Academy of Sciences, 100190 Beijing, China

Ehud Gazit*
Department of Molecular Microbiology and Biotechnology, George S. Wise Faculty of Life Sciences and Department of Materials Science and Engineering Iby and Aladar Fleischman Faculty of Engineering, Tel Aviv University, Tel Aviv 6997801, Israel

Abstract

Conformational transition of proteins and peptides into highly stable, β-sheet-rich structures is observed in many amyloid-associated neurodegenerative disorders, yet the precise mechanism of amyloid formation at the molecular level remains poorly understood due to the complex molecular structures. Short peptides provide simplified models for studying the molecular basis of the assembly mechanism that governs β-sheet fibrillation processes underlying the formation and inhibition of amyloid-like structures. Herein, we report a supramolecular coassembly strategy for the inhibition and transformation of stable β-sheet-rich amyloid-derived dipeptide self-assemblies

Corresponding Authors: jbli@iccas.ac.cn, yanxh@ipe.ac.cn, ehudg@post.tau.ac.il.
The authors declare no competing financial interest.

into adaptable secondary structural fibrillar assemblies by mixing with bipyridine derivatives. The interplay between the type and mixing ratio of bipyridine derivatives allowed the variable coassembly process with stimuli-responsive functional properties, studied by various experimental characterizations and computational methods. Furthermore, the resulting coassemblies showed functional redox- and photoresponsive properties, making them promising candidates for controllable drug release and fluorescent imprint. This work presents a coassembly strategy not only to explore the mechanism of amyloid-like structure formation and inhibition at the molecular level but also to manipulate amyloid-like structures into responsive supramolecular coassemblies for material science and biotechnology applications.

Keywords

amyloid-like structure; self-assembly; dipeptide; stimuli-responsive; supramolecular chemistry

Supramolecular self-assembly of biological macromolecules is a ubiquitous phenomenon in living systems.[1–9] However, the self-assembly of misfolded proteins and peptides into highly ordered β-sheet-rich oligomeric structures and further into fibrillar aggregations, which are known as amyloid fibrils, is associated with various degenerative disorders such as Alzheimer's disease, Parkinson's disease, and type II diabetes.[10–19] The conformational transitions from random coils and α-helix to β-sheet occur during the misfolding processes. However, the precise mechanism of amyloid formation at the molecular level remains poorly understood due to the complex molecular structures of biological proteins and peptides comprising long sequence of amino acid residues and in some cases a mixture of secondary structural conformations.[20–24] To simplify this complexity, significant effort has been devoted to develop suitable models of amyloid-like β-sheet-rich fibrillar structures formed by short peptide fragments,[25–30] allowing us to study the underlying molecular details of conformational changes and potentially setting the basis for rational molecular design of inhibitors as therapeutic agents to treat amyloid-associated disorders.

External stimuli have been utilized to initiate and control the structural transition of model amyloid assembly, including temperature,[31] pH,[32,33] metal ions,[34,35] chemical reactions,[22] and coassembled additives.[36–38] Among these, the coassembly strategy has gained considerable attention due to the specific hydrogen bonding and π-π interactions between amyloidderived peptides and inhibitors that facilitate in-depth understanding of the molecular processes of amyloid formation and inhibition.[39] While the design of multiple responsive molecular self-assemblies by single component molecules is still an unmet challenge in materials science, coassembly provides avenues to fine-tune the stimuli-responsive behavior by readily incorporating functional interacting segments. These modules can undergo physical or chemical conformational changes in response to external stimuli such as pH, light, redox, electricity, and magnetic field.[40–43] Therefore, coassembly with inhibitor molecules could not only disrupt the formation of amyloid-like structures but also generate functional supramolecular materials.

Herein, the extensively studied Fmoc-protected diphenylalanine (FmocFF) dipeptide containing the core recognition FF motif of the Alzheimer's β-amyloid polypeptide was

Europe PMC Funders Author Manuscripts

selected as an ultrashort amyloid model.[44] FmocFF can self-assemble to form highly ordered and stable β-sheet-rich fibrous nanostructures *via* intermolecular hydrogen bonding and aromatic stacking interactions,[45,46] which, similarly to amyloid fibrils, show the characteristic morphology, secondary structure conformation, and Congo red/ThT binding signatures.[47–49] Based on the strong intermolecular hydrogen bonding between pyridine and carboxylic acid,[50] two simple bipyridine derivatives, namely 1,2-bis(4-pyridyl)ethylene (BPE) and 4,4'-dipyridyl disulfide (DPDS), were examined for binding to the carboxylic acid of FmocFF and for manipulation of the conformational change of β-sheet-rich amyloid fibrils (Figure 1). The coassembly between BPE/DPDS and FmocFF was fully investigated by assembly kinetics, mechanical properties analysis, transmission electron microscopy (TEM), power X-ray diffraction (PXRD), Fourier transform infrared (FTIR), and nuclear magnetic resonance (NMR). By fine-tuning the type and molar ratio of bipyridine/dipeptide, a transition of the β-sheet into an unstructured conformation was observed at FmocFF/BPE ratios of 1:0.5 and 1:1 by circular dichroism (CD) and ThT assays, demonstrating reduced amyloid signatures. Furthermore, the molecular mechanism of coassembly and structural transition were studied by density functional theory (DFT) calculations and all-atom molecular dynamics (AAMD) simulations, suggesting intermolecular hydrogen bonding to be the predominant driving force of the formation of new molecular arrangements. Due to the nature of redox- and photoresponsive bipyridine derivatives (BPE/DPDS), responsive gel materials were fabricated by coassembly with FmocFF. These results demonstrate the coassembly induced conformational transition of β-sheet rich amyloid-like structures and provide insights into the design and development of functional coassembled gel materials for future applications in drug delivery, cell culture, and fluorescent imprint.

Results and Discussion

Based on the strong intermolecular hydrogen-bonding interactions between carboxylic acid and pyridine, we selected two bipyridine derivatives and studied the inhibition of amyloid-like structures for FmocFF/BPE and FmocFF/DPDS at three molar ratios (1:0.25, 1:0.5, and 1:1). Gel formation was performed by the "heating-cooling" switch method and assessed by the "inverted-vial" method. The formation of self-supported and invertible gels was observed for all mixture solutions, as well as for FmocFF alone, while no gel was formed by either BPE or DPDS. We further recorded time-lapse optical images during the gel formation and studied the dynamic kinetics of assembly by turbidity change of the solutions (Figure 2a). For FmocFF alone, a transparent−opaque−transparent turbidity change was observed from 0 to 100 s. For FmocFF/BPE at different ratios, a similar turbidity change was observed, though a longer time was required to complete the transparency change (160-210 s). For FmocFF/DPDS at different ratios (Figure S1), the transparent−opaque−transparent transition (except the 1:1 ratio) and higher turbidity were observed for all of the solutions, requiring a longer time for the 1:0.25 and 1:0.5 ratios (150 and 180 s), compared to the 1:1 ratio (60 s). All of the examined solutions formed stable gels after 0.5 h. These results suggest that coassembly indeed occurred in both FmocFF/BPE and FmocFF/DPDS mixtures, and the assembly kinetics was influenced by the ratio of the two components.

Rheology was employed to evaluate the mechanical properties of the FmocFF gel and the FmocFF/pyridine-coassembled gels. The storage (G') and loss modulus (G'') of a

viscoelastic material, representing the deformation energy stored and dissipated during the shear process, respectively, were measured. First, strain sweep experiments were performed to determine the linear viscoelastic regime (LVR) of the hydrogels (Figure 2b and Figure S2). A breakage strain of 40% was observed for the FmocFF hydrogel. Interestingly, the breakage strain of the FmocFF/DPDS hydrogels increased from 53% to 90% by increasing the fraction of DPDS from 1:0.25 to 1:1. However, for the FmocFF/BPE hydrogels, even though the breakage strain increased to 65% at the lower BPE concentration (1:0.25 FmocFF/BPE), a reduction to 30% and 16% was observed for 1:0.5 and 1:1 FmocFF/BPE, respectively. Next, dynamic frequency sweep experiments within the LVR were performed (Figure 2c and Figure S3), allowing us to compare the G' and G'' values of the FmocFF and coassembled hydrogels, thus indicating their mechanical rigidity. The frequency-independent G' and G'' values along with $G' > G''$ established the solid-like nature of the FmocFF and the coassembled hydrogels. Compared to the pure FmocFF gel, the coassembled hydrogels exhibited increased modulus values at every molar ratio, indicating the formation of stiffer coassembled gels. The highest G' value was observed for the 1:1 FmocFF/BPE hydrogels (Figure S3e), although it underwent breakage at the lowest strain value. This behavior may indicate that the FmocFF/BPE coassembled structures are likely more rigid and hence unable to withstand higher strain values. The difference in modulus values indicated different networks of micro/nanostructures inside the gels, potentially influencing their mechanical properties.[52] Therefore, compared to FmocFF self-assembly, FmocFF coassembled with DPDS/BPE to produce improved mechanical properties of the coassembled gels.

To investigate the coassembly effect on FmocFF assembly by the addition of bipyridines, the morphologies of the gels were studied by TEM. Well-defined nanofibrous structures were observed for FmoFF alone, with a statistical fibril width of 21.0 ± 2.2 nm (Figure 2d, Figure S4a). No obvious change of nanofibrils was found for the 1:0.25 FmocFF/BPE gel (Figure 2e, Figure S4b). However, significant morphological transition from nanofibrils to nanorod-like structures was observed by increasing the BPE concentration to either 1:0.5 or 1:1 FmocFF/BPE (Figure 2f,g, Figure S4c,d). The size of the structures was increased compared to that of FmocFF alone, with a width of 37.7 ± 8.9 nm and 82.8 ± 10.6 nm for 1:0.5 and 1:1 FmocFF/BPE, respectively, indicating that coassembly contributed to the mechanical rigidity of the gels as demonstrated in rheology measurements. The FmocFF/DPDS gels showed nanofibrous structures with a slightly increased width compared to FmocFF alone, namely 24.1 ± 2.9, 23.2 ± 3.7, and 21.9 ± 2.3 nm for 1:0.25, 1:0.5, and 1:1 FmocFF/DPDS, respectively (Figure S5).

To further study the coassembly in the two-component gels, we examined the PXRD patterns of hybrid xerogels and individual compounds (Table S1). The BPE alone structures displayed sharp diffraction peaks (14.01° (6.3 Å), 16.66° (5.3 Å), 17.54° (5.1 Å), 20.46°(4.3 Å), 21.28° (4.2 Å), 21.95° (4 Å), 22.63° (3.9 Å), 24.20° (3.7 Å), 26.84° (3.3 Å), 28.20° (3.2 Å), 33.84° (2.6 Å)). However, FmocFF xerogel did not exhibit significant diffraction signals, signifying the amorphous molecular organization. On the other hand, FmocFF/BPE xerogel displayed sharp and intense new low-angle diffraction peaks (7.15° (12.4 Å), 10.88° (8.1 Å) and 13.54° (6.5 Å)) along with the higher-angle BPE signals attributed to the crystalline arrangement of molecules and the preferred orientation of molecular planes within the

coassembled structures. A similar finding was observed in the case of 1:1 FmocFF/DPDS coassembled xerogels (Figure S6). These results demonstrate that new aggregate phases were formed and coassembly indeed occurred in the two-component gels. The formation of intermolecular hydrogen bonding between the carboxylic acid of FmocFF and the pyridine of BPE/DPDS was studied by FTIR and ^{1}H NMR. The FTIR peak at 1746 cm^{-1} was ascribed to the carboxylic acid of FmocFF. This peak was decreased and shifted to 1729 and 1715 cm^{-1} in 1:1 FmocFF/BPE and 1:1 FmocFF/DPDS, respectively, suggesting hydrogen bonding between carboxylic acid and pyridine in the coassembled gels (Figure 2i and Figure S7). In ^{1}H NMR experiments (Figure 2j and Figure S8), the proton signal assigned to the carboxylic acid group of FmocFF was broadened and weakened by adding bipyridines (BPE and DPDS), demonstrating the hydrogen bonding interactions between the carboxylic acid and pyridine.[38]

To explore the potential inhibitory effect of bipyridine derivatives on the formation of amyloid-like β-sheet conformation of FmocFF assembly, CD spectra and higher magnification TEM images of the coassemblies were recorded.[53] One positive and one negative Cotton effects at 193 and 208 nm, respectively, were observed for FmocFF alone, suggesting β-sheet rich self-assemblies (Figure 3a).[54] The flat ribbon-like fibril was also observed in the FmocFF gel (Figure 3b), which was reported in the previous study.[45] The negative peak at 308 nm was assigned to the π-π interactions between Fmoc aromatic groups, which contributed to stabilize the packing of supramolecular self-assemblies. By coassembly with BPE at a 1:0.25 ratio (Figure 3c-d), the intensity of the β-sheet Cotton effect peaks was greatly decreased and slightly red-shifted to 196 and 210 nm, yet still indicating the presence of β-sheet assemblies with ribbon structures inside the sample. Upon further increasing the molar ratio of FmocFF/BPE to 1:0.5 and 1:1, the β-sheet Cotton effect peaks completely vanished (Figure 3e and 3g), demonstrating a secondary structure transition from β-sheet to unstructured conformation as a result of coassembly. Moreover, a significant morphological transition from ribbon-like to rod-like fibril structures was observed for 1:0.5 and 1:1 FmocFF/BPE (Figure 3f and 3h). The red-shifted negative peaks (321-331 nm) for π-π interactions between the Fmoc aromatic groups were found for the three ratios of FmocFF/BPE coassemblies. In contrast, the nature of the β-sheet conformation of FmoccFF was not changed after coassembly with DPDS at the three molar ratios (Figure 3i-j and Figure S9), with the positive and negative Cotton effects of ribbon structures showing a different shift for 1:0.25 FmocFF/DPDS (192, 212 nm), 1:0.5 FmocFF/DPDS (192, 204 nm), and 1:1 FmocFF/DPDS (194, 206 nm). No assembly was observed for either BPE or DPDS alone (Figure 3k-l). Peak separation calculations were carried out through peak fitting of FTIR spectrum and the proportion of estimated secondary structures is obtained in Figure S10. For individual FmocFF, 59.9% of β-sheet conformation (1695 cm^{-1}) and 40.1% of disordered conformation (1655 cm^{-1}) was observed. However, the lower proportion of β-sheet was found in the coassemblies of 1:1 FmocFF/BPE (30.3%, 1690 cm^{-1}) and 1:1 FmocFF/DPDS (50.1%, 1703 cm^{-1}), the shifted peaks indicated the new arrangement of β-sheet conformation in the coassemblies.

To further study the inhibition of amyloid fibrils by coassembly, assays employing Thioflavin T (ThT), a commonly used indicator to quantify amyloid fibrils,[55] were performed. Upon binding to amyloid fibrils, ThT exhibits an enhanced fluorescence signal at

482 nm under excitation at 450 nm. As shown in Figure 3m,n, no fluorescence was detected for all the gels without the addition of ThT. However, significantly enhanced fluorescence was observed for the FmocFF gel in the presence of ThT, indicating the formation of β-sheet-rich amyloid-like fibrils. The intensity of ThT fluorescence was greatly decreased in the coassembled gels upon increasing the amount of bipyridines, thus demonstrating the inhibition of amyloid-like structure formation in the presence of BPE and DPDS. The β-sheet conformation of FmocFF/DPDS coassembly showed lower amyloid signature compared to the FmocFF self-assembly. Compared to the strong ThT fluorescence observed for FmocFF fibrils, the coassembled fibrous structures displayed decreased green emission, as observed by fluorescence microscopy (Figure 3o,p and Figure S11).

To gain further insight into the inhibition mechanism of the FmocFF β-sheet-rich structure through coassembly with BPE, DFT calculations and AAMD simulations were performed, allowing us to analyze the intermolecular interactions and molecular organizations between FmocFF (Figure S12) and BPE molecules. FmocFF/BPE dimers connected through different types of hydrogen bonds were first constructed and optimized by the DFT calculations (Figure 4a), indicating that strong hydrogen-bonding interactions dominate the dimers. Moreover, the dimer connected through an O-H···N hydrogen bond between carboxylic acid and pyridine showed the strongest binding energy, consistent with the experiment results (Table S2). It should be noted that an FmocFF/BPE trimer stabilized by O-H···N hydrogen bonds also exhibited the largest binding energy (Figure 4b and Figure S13). Therefore, the strong intermolecular hydrogen-bonding interactions between FmocFF and BPE would affect the molecular arrangements of FmocFF and further induce the structural transition. Next, we explored the effect of BPE on the molecular organization of FmocFF through AAMD simulations by tracking the dynamic evolution of FmocFF self-assembly as well as FmocFF/BPE coassembly. Tightly packed and stable assemblies of FmocFF were found to form after a 100 ns AAMD simulation, comprising β-sheet hydrogen bonds between the amide groups of FmocFF (Figure 4c and Figure S14). In the presence of BPE, however, an entangled network of FmocFF and BPE was observed due to the driving force of intermolecular hydrogen-bonding interactions (Figure 4d, left). Further insights into the molecular arrangements of FmocFF within the coassemblies demonstrated a loose molecular stacking network (Figure 4d, right), which is distinct from the dense packing modes of individual FmocFF assemblies. Moreover, comparison between the typical FmocFF clusters in self-assemblies versus coassemblies revealed that the classical β-sheet hydrogen bonds between FmocFF molecules were inhibited and random hydrogen bonds formed between FmocFF, inducing the secondary structure transformation of FmocFF assemblies (Figure 4e and Figure S14).

We further studied the stimuli-responsive properties of the two coassembled gels following the incorporation of functional bipyridines. Disulfide bonds have been widely used as a redox-responsive linkage that can be specifically cleaved by redox agents through thiol-disulfide exchange reactions,[56] such as 1,4-dithio-DL-threitol (DTT), glutathione (GSH), and tris(2-carboxyethyl) phosphine (TCEP). Notably, the concentration of GSH, a cellular reducing tripeptide, is 2-10 mM in tumor cells, 100-1000 times higher than the extracellular concentration (~ 2-20 μM) and at least 4-fold higher compared to normal cells.[57] Therefore, much effort has been put into the development of different disulfide-containing nanovehicles

(*e.g.*, polymeric hydrogels) for controllable drug release in tumor cells, based on their high reducing potential. The potentially promising of fabricating redox responsive gels by simple organic molecules through supramolecular assembly has so far remained poorly explored. The redox-response reaction of disulfide-containing DPDS in the presence of GSH is depicted in Figure 5a. The disulfide bond of DPDS is cleaved by GSH to produce disulfide-containing oxidized glutathione (GSSH) and 4-mercaptopyridine (PS), as confirmed by ^{1}H NMR and mass spectrometry (MS) spectra. The Ha and Hb of DPDS and the Hc of GSH decreased and almost disappeared by adding increasing amounts of GSH up to a molar ratio of 1:2 DPDS/GSH, with a new upfield shifted peak of Ha′ and downfield shifted peaks of Hb′ and Hc′ observed for PS and GSSH (Figure 5b). MS spectra of 1:2 DPDS/GSH showed strong new peaks at *m*/*z* 111.9 and 613.3, further confirming the production of PS and GSSH. Moreover, the UV-vis absorption spectrum of DPDS exhibited two absorption peaks at 289 and 253 nm, which decreased significantly at 1:1 and 1:2 DPDS/GSH (Figure S15). A strong new peak at 337 nm was ascribed to the absorption peak characteristic of PS,[58] indicating the occurrence of thiol−disulfide exchange reactions. Due to the redox-responsiveness of molecular DPDS, we further studied the redox-sensitivity of the coassembled FmocFF/DPDS gel in a reductive environment. As shown in Figure 5d, increasing transparency of the coassembled gel was observed over 4 h following the addition of 1 mL PBS buffer containing the GSH reducing agent on top of the gel, while the coassembled gel kept stable with observed no transparency change in PBS without GSH. Furthermore, individual FmocFF gel cannot be dis-assembled in the presence of redox agent (Figure S16). A suggested mechanism of the coassembly and disassembly of the FmocFF/DPDS gel is shown in Figure 5e. FmocFF and DPDS coassemble and form supramolecular packing networks through intermolecular hydrogen bonding. After the disulfide cleavage by GSH, DPDS is transformed into PS and the intermolecular hydrogen bonding is broken, inducing the network disassembly. TEM images of the FmocFF/DPDS gel networks before and after the addition of the reducing agent also confirmed the disassembly of the entangled nanofibrils after dithiol−disulfide exchange reactions (Figure S17). The redox-responsive property of the FmocFF/DPDS coassembled gel holds potential applications in drug encapsulation and controllable release (Figure S18).

Photoresponsive materials have gained increasing interest in optical and biological fields since light allows noncontact remote control on the temporal and spatial resolution of the response.[59] Various photochromic groups have been incorporated into polymeric and supramolecular materials that in response to light undergo a cis-trans isomerization to serve as optical and photoelectric switches.[60] We investigated the UV light responsiveness of molecular BPE with a similar structure of photochromic stilbene derivatives61 by UV-vis absorption and fluorescence spectra (Figure 5f). The absorption intensity of BPE decreased over the time of UV light irradiation at 365 nm, indicating a photodegradable property (Figure S19). Very weak fluorescence was detected before UV light irradiation, while the fluorescence intensity was significantly increased in the blue emission range after 90 min of UV light irradiation, suggesting enhanced fluorescence during the cis-trans isomerization (Figure 5g). The steric hindrance of cis-BPE with a smaller dihedral angle hinders and restricts the free rotation of the ethylene bond, resulting in enhanced fluorescence.[62] We next explored the photoresponsiveness of BPE in the Fmoc-FF/BPE

coassembled gel (Figure 5h). Before UV irradiation, the coassembled gel showed no visible fluorescence under a 365 nm excitation. Interestingly, significantly enhanced fluorescence was imprinted in the coassembled gel using a star-shaped photomask of tinfoil after 1 h UV light irradiation. As a control, individual FmocFF hydrogel could not be imprinted after 1 h of UV light irradiation (Figure S20). Furthermore, the coassembled gel exhibited a self-erasing property after 3 days, indicating potential applications of BPE-containing coassembled gels in rewritable fluorescent patterning. The biocompatibility of the FmocFF/BPE and FmocFF/DPDS coassemblies was also evaluated *via* an 2,3-bis(2-methoxy-4-nitro-5-sulfophenyl)-2H-tetrazolium-5-carboxanilide (XTT)-based cell viability assay for the 3T3 mouse fibroblast cell line (Figure S21). After culturing for 24 h, over 90% of the 3T3 mouse fibroblast cells survived, demonstrating the good biocompatibility of FmocFF based assemblies.

Conclusion

In summary, we report the coassembly directed inhibition and secondary structure transformation of amyloid-like β-sheet-rich dipeptide nanofibrils through intermolecular hydrogen bonding between bipyridines and dipeptides. The coassembly and induced conformational transition from β-sheet to unstructured stacking were fully studied by various experimental characterizations and computational methods. Furthermore, the coassemblies exhibit redox- and photoresponsive properties due to the incorporated functional bipyridines, making them promising candidates for future applications in controllable drug release and fluorescent patterning. The present work not only provides insights into the mechanism of the formation and inhibition of amyloid-like structures at the molecular level using short peptide models, but also provides a proof-of-concept strategy to manipulate amyloid-like structures into smart responsive materials.

Methods

Gel Preparation

A “heating-cooling” method was used for gel preparation. The powder of FmocFF, FmocFF/BPE, or FmocFF/DPDS was dissolved in water containing 30% methanol by heating at a final concentration of 2.0 mg/mL. After cooling for several hours at ambient temperature, gel formation was observed. The total gelator concentration was 2.0 mg/mL. Gel formation was evaluated by the “inverted-vial” method showing that the gel can support its own weight against gravity.

TEM Analysis

Hydrogel samples of 20 μL were drop-casted onto a glow discharge copper grid (400 mesh), coated with thin carbon film and absorbed for 2 min. Excess sample solution was removed, and the copper grid was washed three times with deionized water and stained with one drop of 2.0% (w/v) uranyl acetate for 2 min. TEM images were viewed using a JEOL 1200EX electron microscope operating at 80 kV.

Powder X-ray Diffraction (PXRD)

PXRD patterns of the dried gels were recorded using a BRUKER d8 Advance diffractometer equipped with Goebels mirrors to parallelize the beam and LYNXEYE-XE linear detector.

FTIR Spectroscopy

To obtain the FTIR spectra, 50 μL of each gel was deposited onto a real crystal KBr IR card (International Crystal Laboratories, Garfield, NJ) and allowed to dry under vacuum overnight. The dried sample was then wetted with 500 μL of D_2O three times. The FTIR spectra were recorded on a Nicolet 6700 FTIR spectrometer (Thermo Scientific, Waltham, MA), from 1800 to 1500 cm^{-1}, at room temperature. The background baseline was recorded using D_2O and subtracted to obtain each FTIR spectrum. The FTIR spectra were fitted by multiple Gaussian peaks, and the estimated proportion of secondary structure constituent was calculated using the OriginPro software.

CD Spectroscopy

CD spectra of all of the gels were recorded on an Applied Photophysics Chirascan spectrometer with a bandwidth of 1.0 nm in the ultraviolet (UV) region (190-350 nm) using a 0.1 mm quartz cuvette. All of the scans were carried out at a scan speed of 50 nm/min with a data pitch of 0.5 nm at room temperature. All spectra were obtained following solvent background subtraction. The reported spectra represent the average of three scans.

Supplementary Material

Refer to Web version on PubMed Central for supplementary material.

Acknowledgments

This work was supported by the European Research Council under the European Union Horizon 2020 research and innovation program (No. 694426) (E.G.), National Natural Science Foundation of China (Project Nos. 21522307, 21773248, 21802144, and 21802143), the National Natural Science Fund BRICS STI Framework Programme (No. 51861145304), and Innovation Research Community Science Fund (No. 21821005) as well as the Key Research Program of Frontier Sciences of the Chinese Academy of Sciences (CAS, Grant No. QYZDB-SSW-JSC034) (X.Y.). The authors thank Dr. Sigal Rencus-Lazar for language editing assistance.

References

(1). Whitesides GM, Mathias JP, Seto CT. Molecular Self-Assembly and Nanochemistry: A Chemical Strategy for the Synthesis of Nanostructures. Science. 1991; 254: 1312–1319. [PubMed: 1962191]

(2). Zhang S. Fabrication of Novel Biomaterials through Molecular Self-Assembly. Nat Biotechnol. 2003; 21: 1171–1178. [PubMed: 14520402]

(3). Aida T, Meijer EW, Stupp SI. Functional Supramolecular Polymers. Science. 2012; 335: 813–817. DOI: 10.1126/science.1205962 [PubMed: 22344437]

(4). Lampel A, Ulijn RV, Tuttle T. Guiding Principles for Peptide Nanotechnology through Directed Discovery. Chem Soc Rev. 2018; 47: 3737–3758. [PubMed: 29748676]

(5). Wang HM, Feng ZQQ, Xu B. Bioinspired Assembly of Small Molecules in Cell Milieu. Chem Soc Rev. 2017; 46: 2421–2436. DOI: 10.1039/c6cs00656f [PubMed: 28357433]

(6). Dou XQ, Feng CL. Amino Acids and Peptide-Based Supramolecular Hydrogels for Three-Dimensional Cell Culture. Adv Mater. 2017; 29 [PubMed: 28112836]

(7). Ji W, Xue B, Arnon ZA, Yuan H, Bera S, Li Q, Zaguri D, Reynolds NP, Li H, Chen Y, Gilead S, et al. Rigid Tightly Packed Amino Acid Crystals as Functional Supramolecular Materials. ACS Nano. 2019; 13: 14477–14485. [PubMed: 31755683]

(8). Yuan C, Ji W, Xing RR, Li JB, Gazit E, Yan XH. Hierarchically Oriented Organization in Supramolecular Peptide Crystals. Nat Rev Chem. 2019; 3: 567–588.

(9). Jia X, Minami K, Uto K, Chang AC, Hill JP, Ueki T, Nakanishi J, Ariga K. Modulation of Mesenchymal Stem Cells Mechanosensing at Fluid Interfaces by Tailored Self-Assembled Protein Monolayers. Small. 2019; 15 [PubMed: 30624030]

(10). Stefani M, Dobson CM. Protein Aggregation and Aggregate Toxicity: New Insights into Protein Folding, Misfolding Diseases and Biological Evolution. J Mol Med. 2003; 81: 678–699. [PubMed: 12942175]

(11). Dong JJ, Shokes JE, Scott RA, Lynn DG. Modulating Amyloid Self-Assembly and Fibril Morphology with Zn(II). J Am Chem Soc. 2006; 128: 3540–3542. DOI: 10.1021/ja055973j [PubMed: 16536526]

(12). Knowles TP, Vendruscolo M, Dobson CM. The Amyloid State and Its Association with Protein Misfolding Diseases. Nat Rev Mol Cell Biol. 2014; 15: 384–396. [PubMed: 24854788]

(13). Knowles TPJ, Mezzenga R. Amyloid Fibrils as Building Blocks for Natural and Artificial Functional Materials. Adv Mater. 2016; 28: 6546–6561. [PubMed: 27165397]

(14). Adamcik J, Mezzenga R. Amyloid Polymorphism in the Protein Folding and Aggregation Energy Landscape. Angew Chem, Int Ed. 2018; 57: 8370–8382. [PubMed: 29446868]

(15). Ke PC, Sani M-C, Ding F, Kakinen A, Javed I, Separovic F, Davis TP, Mezzenga R. Implications of Peptide Assemblies in Amyloid Diseases. Chem Soc Rev. 2017; 46: 6492–6531. DOI: 10.1039/c7cs00372b [PubMed: 28702523]

(16). Jin Y, Sun Y, Lei J, Wei G. Dihydrochalcone Molecules Destabilize Alzheimer's Amyloid-β Protofibrils through Binding to the Protofibril Cavity. Phys Chem Chem Phys. 2018; 20: 17208–17217. [PubMed: 29900443]

(17). Lao Z, Chen Y, Tang Y, Wei G. Molecular Dynamics Simulations Reveal the Inhibitory Mechanism of Dopamine against Human Islet Amyloid Polypeptide (hIAPP) Aggregation and Its Destabilization Effect on hIAPP Protofibrils. ACS Chem Neurosci. 2019; 10: 4151–4159. [PubMed: 31436406]

(18). Mason TO, Shimanovich U. Fibrous Protein Self-Assembly in Biomimetic Materials. Adv Mater. 2018; 30 [PubMed: 29883013]

(19). Wang ST, Lin YY, Spencer RK, Thomas MR, Nguyen AI, Amdursky N, Pashuck ET, Skaalure SC, Song CY, Parmar PA, Morgan RM, et al. Sequence-Dependent Self-Assembly and Structural Diversity of Islet Amyloid Polypeptide-Derived β-Sheet Fibrils. ACS Nano. 2017; 11: 8579–8589. DOI: 10.1021/acsnano.7b02325 [PubMed: 28771324]

(20). Xu Y, Shen J, Luo X, Zhu W, Chen K, Ma J, Jiang H. Conformational Transition of Amyloid β-Peptide. Proc Natl Acad Sci U S A. 2005; 102: 5403–5407. DOI: 10.1073/pnas.0501218102 [PubMed: 15800039]

(21). Pagel K, Koksch B. Following Polypeptide Folding and Assembly with Conformational Switches. Curr Opin Chem Biol. 2008; 12: 730–739. [PubMed: 18840544]

(22). Mimna R, Camus M-S, Schmid A, Tuchscherer G, Lashuel HA, Mutter M. Disruption of Amyloid-Derived Peptide Assemblies through the Controlled Induction of a β-Sheet to α-Helix Transformation: Application of the Switch Concept. Angew Chem, Int Ed. 2007; 46: 2681–2684. [PubMed: 17330907]

(23). Gilead S, Gazit E. Self-Organization of Short Peptide Fragments: From Amyloid Fibrils to Nanoscale Supramolecular Assemblies. Supramol Chem. 2005; 17: 87–92.

(24). Davies RPW, Aggeli A, Beevers AJ, Boden N, Carrick LM, Fishwick CWG, McLeish TCB, Nyrkova IA, Semenov AN. Self-Assembling β-Sheet Tape Forming Peptides. Supramol Chem. 2006; 18: 435–443.

(25). Tenidis K, Waldner M, Bernhagen J, Fischle W, Bergmann M, Weber M, Merkle ML, Voelter W, Brunner H, Kapurniotu A. Identification of a Penta- and Hexapeptide of Islet Amyloid Polypeptide (Iapp) with Amyloidogenic and Cytotoxic Properties. J Mol Biol. 2000; 295: 1055–1071. [PubMed: 10656810]

(26). Reches M, Porat Y, Gazit E. Amyloid Fibril Formation by Pentapeptide and Tetrapeptide Fragments of Human Calcitonin. J Biol Chem. 2002; 277: 35475–35480. [PubMed: 12095997]

(27). Lynn DG, Meredith SC. Model Peptides and the Physicochemical Approach to β-Amyloids. J Struct Biol. 2000; 130: 153–173. [PubMed: 10940223]

(28). Brahmachari S, Arnon ZA, Frydman-Marom A, Gazit E, Adler-Abramovich L. Diphenylalanine as a Reductionist Model for the Mechanistic Characterization of β-Amyloid Modulators. ACS Nano. 2017; 11: 5960–5969. [PubMed: 28575577]

(29). Gour N, Kanth PC, Koshti B, Kshtriya V, Shah D, Patel S, Agrawal-Rajput R, Pandey MK. Amyloid-Like Structures Formed by Single Amino Acid Self-Assemblies of Cysteine and Methionine. ACS Chem Neurosci. 2019; 10: 1230–1239. [PubMed: 30380833]

(30). Shaham-Niv S, Rehak P, Zaguri D, Levin A, Adler-Abramovich L, Vuković L, Kral P, Gazit E. Differential Inhibition of Metabolite Amyloid Formation by Generic Fibrillation-Modifying Polyphenols. Commun Chem. 2018; 1: 25.

(31). Pochan DJ, Schneider JP, Kretsinger J, Ozbas B, Rajagopal K, Haines L. Thermally Reversible Hydrogels via Intramolecular Folding and Consequent Self-Assembly of a de Novo Designed Peptide. J Am Chem Soc. 2003; 125: 11802–11803. [PubMed: 14505386]

(32). Ozbas B, Kretsinger J, Rajagopal K, Schneider JP, Pochan DJ. Salt-Triggered Peptide Folding and Consequent Self-Assembly into Hydrogels with Tunable Modulus. Macromolecules. 2004; 37: 7331–7337.

(33). Xing R, Yuan C, Li S, Song J, Li J, Yan X. Charge-Induced Secondary Structure Transformation of Amyloid-Derived Dipeptide Assemblies from β-Sheet to α-Helix. Angew Chem Int Ed. 2018; 57: 1537–1542. [PubMed: 29266653]

(34). Wang F, Feng CL. Metal-Ion-Mediated Supramolecular Chirality of L-Phenylalanine Based Hydrogels. Angew Chem, Int Ed. 2018; 57: 5655–5659. [PubMed: 29571216]

(35). Ji W, Yuan C, Zilberzwige-Tal S, Xing R, Chakraborty P, Tao K, Gilead S, Yan X, Gazit E. Metal-Ion Modulated Structural Transformation of Amyloid-Like Dipeptide Supramolecular Self-Assembly. ACS Nano. 2019; 13: 7300–7309. [PubMed: 31181152]

(36). Li J, Du XW, Hashim S, Shy A, Xu B. Aromatic-Aromatic Interactions Enable α-Helix to β-Sheet Transition of Peptides to Form Supramolecular Hydrogels. J Am Chem Soc. 2017; 139: 71–74. DOI: 10.1021/jacs.6b11512 [PubMed: 27997165]

(37). Li J, Zhan Z, Du X, Wang J, Hong B, Xu B. Selection of Secondary Structures of Heterotypic Supramolecular Peptide Assemblies by an Enzymatic Reaction. Angew Chem, Int Ed. 2018; 57: 11716–11721. DOI: 10.1002/anie.201806992 [PubMed: 29971927]

(38). Ji W, Yuan CQ, Chakraborty P, Gilead S, Yan XH, Gazit E. Stoichiometry-Controlled Secondary Structure Transition of Amyloid-Derived Supramolecular Dipeptide Co-Assemblies. Commun Chem. 2019; 2: 65.

(39). Makam P, Gazit E. Minimalistic Peptide Supramolecular Co-Assembly: Expanding the Conformational Space for Nanotechnology. Chem Soc Rev. 2018; 47: 3406–3420. DOI: 10.1039/c7cs00827a [PubMed: 29498728]

(40). Gröschel AH, Walther A, Löbling TI, Schacher FH, Schmalz H, Müller AHE. Guided Hierarchical Co-Assembly of Soft Patchy Nanoparticles. Nature. 2013; 503: 247–251. [PubMed: 24185010]

(41). Shafranek RT, Millik SC, Smith PT, Lee C, Boydston AJ, Nelson A. Stimuli-Responsive Materials in Additive Manufacturing. Prog Polym Sci. 2019; 93: 36–67.

(42). Chivers PRA, Smith DK. Shaping and Structuring Supramolecular Gels. Nat Rev Mater. 2019; 4: 463–478.

(43). Jia X, Minami K, Uto K, Chang A, Hill J, Nakanishi J, Ariga K. Adaptive Liquid Interfacially Assembled Protein Nanosheets for Guiding Mesenchymal Stem Cell Fate. Adv Mater. 2020; 32 [PubMed: 31814174]

(44). Reches M, Gazit E. Casting Metal Nanowires within Discrete Self-Assembled Peptide Nanotubes. Science. 2003; 300: 625–627. [PubMed: 12714741]

(45). Smith AM, Williams RJ, Tang C, Coppo P, Collins RF, Turner ML, Saiani A, Ulijn RV. Fmoc-Diphenylalanine Self Assembles to a Hydrogel via a Novel Architecture Based on π-π Interlocked β-Sheets. Adv Mater. 2008; 20: 37–41.

(46). Mahler A, Reches M, Rechter M, Cohen S, Gazit E. Rigid, Self-Assembled Hydrogel Composed of a Modified Aromatic Dipeptide. Adv Mater. 2006; 18: 1365–1370.

(47). Reches M, Gazit E. Self-Assembly of Peptide Nanotubes and Amyloid-Like Structures by Charged-Termini-Capped Diphenylalanine Peptide Analogues. Isr J Chem. 2005; 45: 363–371.

(48). Jacob R, Ghosh D, Singh PK, Basu SK, Jha NN, Das S, Sukul PK, Patil S, Sathaye S, Kumar A, Chowdhury A, et al. Self-Healing Hydrogels Composed of Amyloid Nano Fibrils for Cell Culture and Stem Cell Differentiation. Biomaterials. 2015; 54: 97–105. [PubMed: 25907043]

(49). Diaferia C, Ghosh M, Sibillano T, Gallo E, Stornaiuolo M, Giannini C, Morelli G, Adler-Abramovich L, Accardo A. Fmoc-FF and Hexapeptide-Based Multicomponent Hydrogels as Scaffold Materials. Soft Matter. 2019; 15: 487–496. [PubMed: 30601569]

(50). Bhogala BR, Nangia A. Cocrystals of 1,3,5-Cyclo-hexanetricarboxylic Acid with 4,4‘-Bipyridine Homologues: Acid···Pyridine Hydrogen Bonding in Neutral and Ionic Complexes. Cryst Growth Des. 2003; 3: 547–554.

(51). Crescenzi O, Tomaselli S, Guerrini R, Salvadori S, D’Ursi AM, Temussi PA, Picone D. Solution Structure of the Alzheimer Amyloid Beta-Peptide (1-42) in an Apolar Microenvironment. Eur J Biochem. 2002; 269: 5642–6548. [PubMed: 12423364]

(52). Colquhoun C, Draper ER, Schweins R, Marcello M, Vadukul D, Serpell LC, Adams DJ. Controlling the Network Type in Self-Assembled Dipeptide Hydrogels. Soft Matter. 2017; 13: 1914–1919. [PubMed: 28186211]

(53). Ji W, Zhang S, Yukawa S, Onomura S, Sasaki T, Miyazawa K, Zhang Y. Regulating Higher-Order Organization through the Synergy of Two Self-Sorted Assemblies. Angew Chem, Int Ed. 2018; 57: 3636–3640. [PubMed: 29411922]

(54). Zhang YK, Zhang H, Zou QL, Xing RR, Jiao TF, Yan XH. An Injectable Dipeptide-Fullerene Supramolecular Hydrogel for Photodynamic Antibacterial Therapy. J Mater Chem B. 2018; 6: 7335–7342. [PubMed: 32254642]

(55). Khurana R, Coleman C, Ionescu-Zanetti C, Carter SA, Krishna V, Grover RK, Roy R, Singh S. Mechanism of Thioflavin-T Binding to Amyloid Fibrils. J Struct Biol. 2005; 151: 229–238. [PubMed: 16125973]

(56). Ganta S, Devalapally H, Shahiwala A, Amiji M. A Review of Stimuli-Responsive Nanocarriers for Drug and Gene Delivery. J Controlled Release. 2008; 126: 187–204. [PubMed: 18261822]

(57). Khorsand B, Lapointe G, Brett C, Oh JK. Intracellular Drug Delivery Nanocarriers of Glutathione-Responsive Degradable Block Copolymers Having Pendant Disulfide Linkages. Biomacromolecules. 2013; 14: 2103–2111. [PubMed: 23647437]

(58). Wang Y, Ruan W, Zhang J, Yang B, Xu W, Zhao B, Lombardi JR. Direct Observation of Surface-Enhanced Raman Scattering in ZnO Nanocrystals. J Raman Spectrosc. 2009; 40: 1072–1077.

(59). Jochum FD, Theato P. Temperature- and Light-Responsive Smart Polymer Materials. Chem Soc Rev. 2013; 42: 7468–7483. [PubMed: 22868906]

(60). Ko CC, Yam VWW. Coordination Compounds with Photochromic Ligands: Ready Tunability and Visible Light-Sensitized Photochromism. Acc Chem Res. 2018; 51: 149–159. [PubMed: 29265804]

(61). Marturano V, Cerruti P, Giamberini M, Tylkowski B, Ambrogi V. Light-Responsive Polymer Micro-and Nano-Capsules. Polymers. 2017; 9: 8. doi: 10.3390/polym9010008 [PubMed: 30970685]

(62). Xing P, Chen H, Xiang H, Zhao Y. Selective Coassembly of Aromatic Amino Acids to Fabricate Hydrogels with Light Irradiation-Induced Emission for Fluorescent Imprint. Adv Mater. 2018; 30: 1705633–1705643. [PubMed: 29226605]

Europe PMC Funders Author Manuscripts

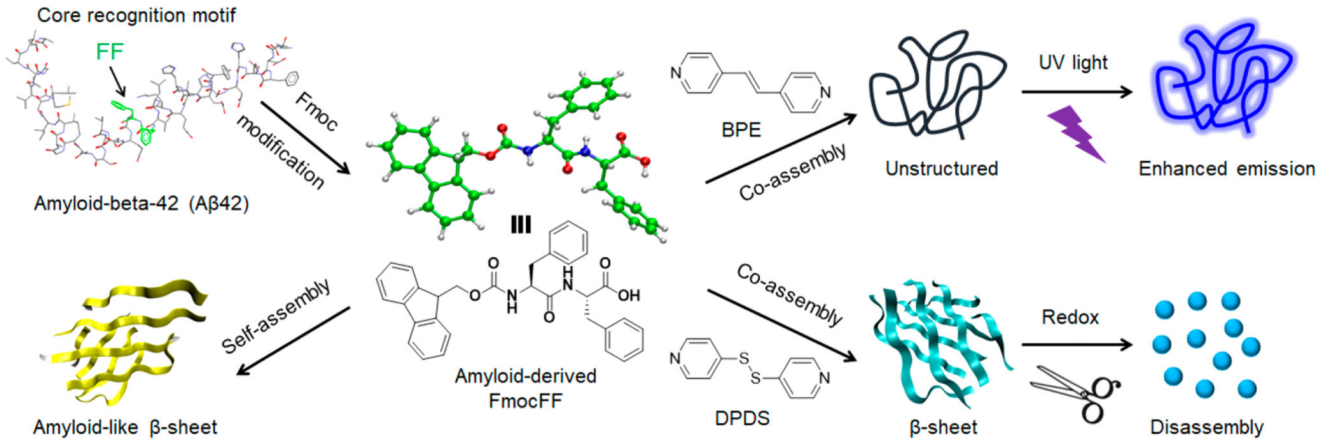

Figure 1.

Schematic presentation of coassembly modulated secondary structure transformation of FmocFF amyloid-like self-assembly into stimuli-responsive supramolecular materials by functional bipyridine derivatives (BPE and DPDS). Molar ratios of 1:1 FmocFF to BPE or DPDS are depicted in the scheme. The ID number of amyloid-beta-42 structure is PDB 1IYT.[51]

Europe PMC Funders Author Manuscripts

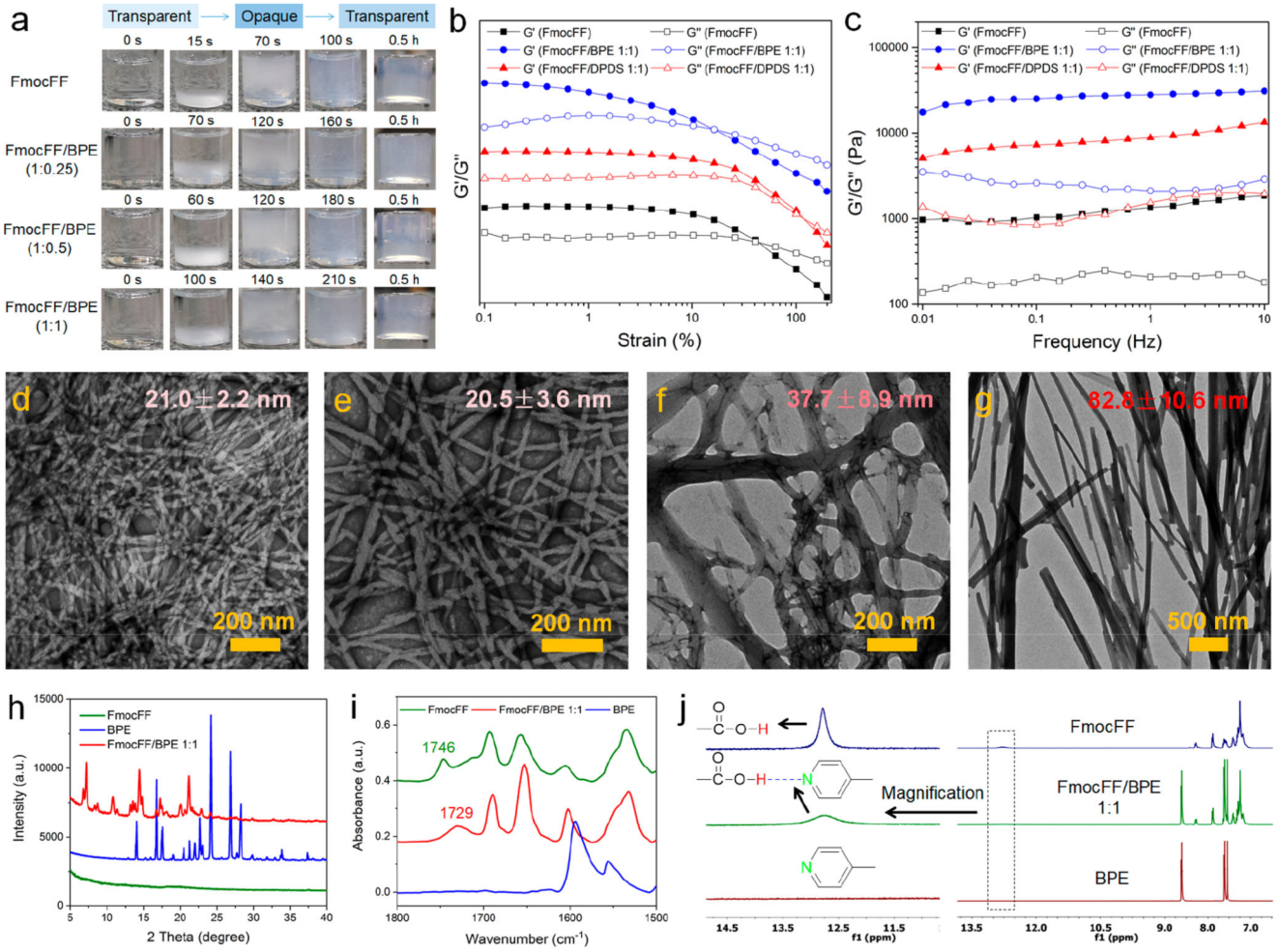

Figure 2.

(a) Time lapse optical images of FmocFF, 1:0.25 FmocFF/BPE, 1:0.5 FmocFF/BPE, and 1:1 FmocFF/BPE. (b) Rheological measurements of dynamic frequency sweep of the FmocFF gel and the 1:1 FmocFF/BPE and 1:1 FmocFF/DPDS coassembled gels at a strain of 0.1% over a range of 0.01−10 Hz. (c) Rheological measurements of dynamic strain sweep of the FmocFF gel and the 1:1 FmocFF/BPE and 1:1 FmocFF/DPDS coassembled gels at a constant frequency of 1 Hz over a strain range of 0.1%−200%. (d−g) TEM images of (d) FmocFF gel, (e) 1:0.25 FmocFF/BPE, (f) 1:0.5 FmocFF/BPE, and (g) 1:1 FmocFF/BPE. The statistical average diameters of the nanofibrils in each gel are indicated. Scale bar is 200 nm. (h) PXRD patterns of the FmocFF gel, BPE powder, and 1:1 FmocFF/BPE gel. (i) FTIR spectra of the FmocFF gel, BPE powder, and 1:1 FmocFF/BPE gel. (j) ^{1}H NMR spectra of FmocFF alone, BPE alone, and the 1:1 FmocFF/BPE mixture in DMSO-d_6. The left part is the proton signal of COOH corresponding to the right spectra after magnification.

Europe PMC Funders Author Manuscripts

Europe PMC Funders Author Manuscripts

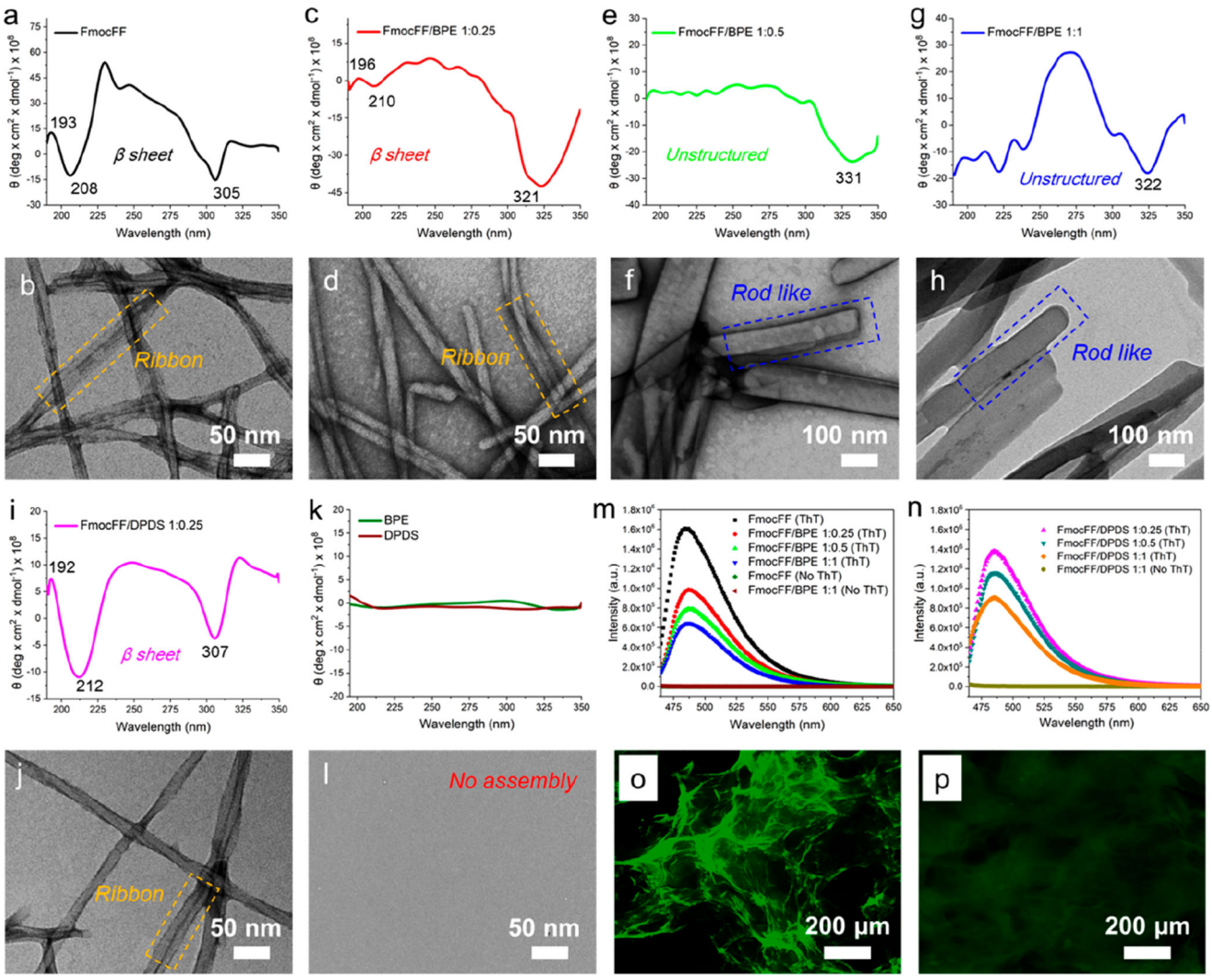

Figure 3.

(a−1) CD spectra and higher magnification TEM images of the FmocFF gel and coassembled FmocFF gels at a concentration of 2 mg/mL. (a, b) FmocFF, (c, d) 1:0.25 FmocFF/BPE, (e, f) 1:0.5 FmocFF/BPE, (g, h) 1:1 FmocFF/BPE, (i, j) 1:0.25 FmocFF/DPDS, (k, l) BPE and DPDS alone. (m) Fluorescence emission of FmocFF and FmocFF/BPE at different molar ratios with and without ThT excited at 450 nm. (n) Fluorescence emission of FmocFF/DPDS at different molar ratios with and without ThT excited at 450 nm. (o, p) Fluorescence microscopy images of (o) FmocFF and (p) FmocFF/BPE (1:1) assembled structures incubated with ThT.

Europe PMC Funders Author Manuscripts

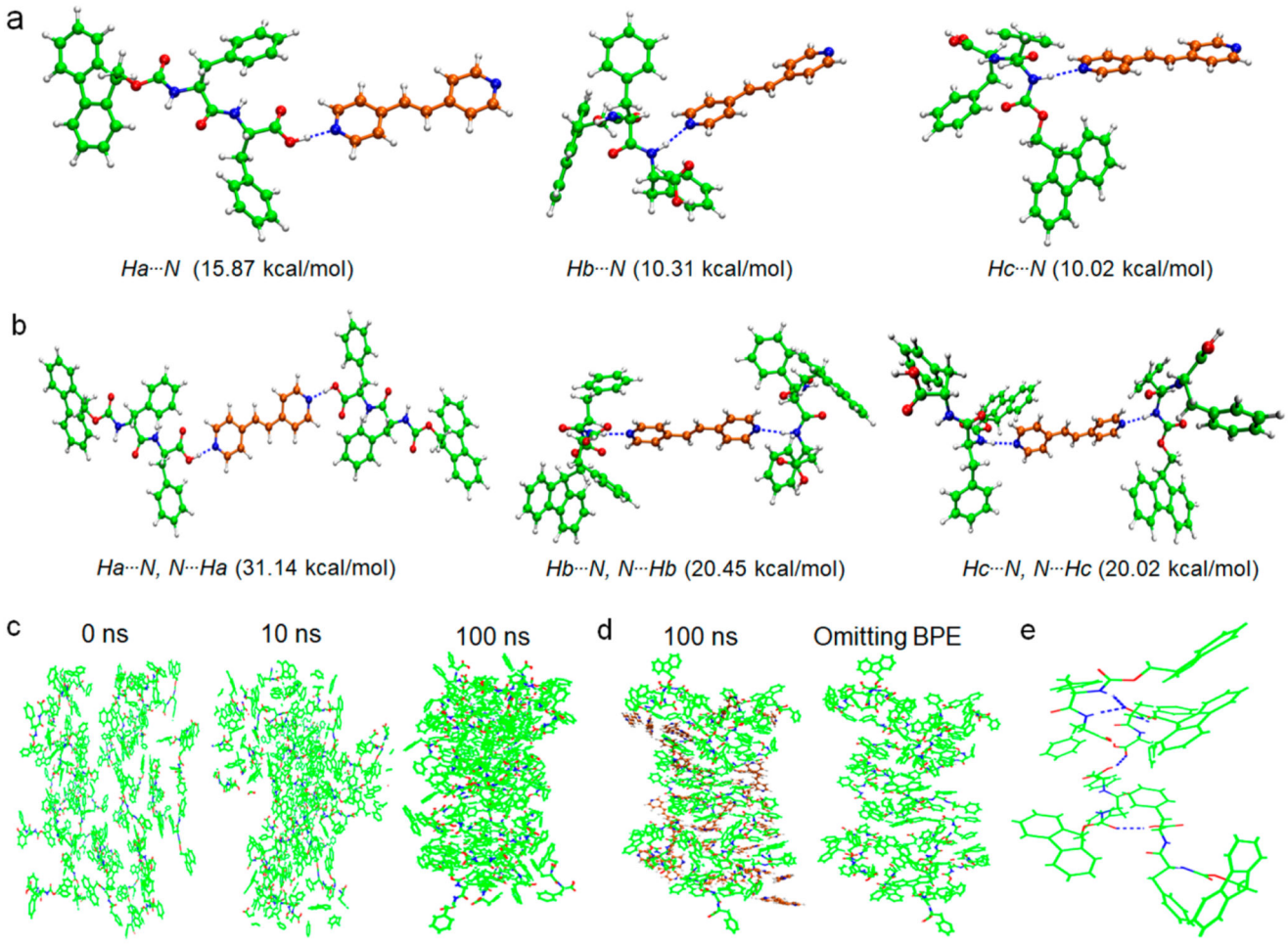

Figure 4.

Multiple (a) dimers and (b) trimers of FmocFF and BPE connected by different hydrogen-bonding interaction modes, as demonstrated by DFT calculations. Corresponding binding energy of FmocFF/BPE is shown below the molecular packing patterns. (c) Snapshots of FmocFF assemblies at different intervals obtained from AAMD simulations from 0 to 100 ns. (d) Snapshot of stable FmocFF/BPE coassemblies after AAMD simulations at 100 ns (left); molecular arrangements of FmocFF within the coassemblies after omitting BPE molecules (right). (e) Typical molecular cluster showing the intermolecular hydrogen bonds between FmocFF molecules in FmocFF/BPE coassemblies. The dashed blue lines denote the intermolecular hydrogen bonds between FmocFF molecules. The carbon atoms in FmocFF and BPE molecules are labeled in green and brown, respectively.

Europe PMC Funders Author Manuscripts

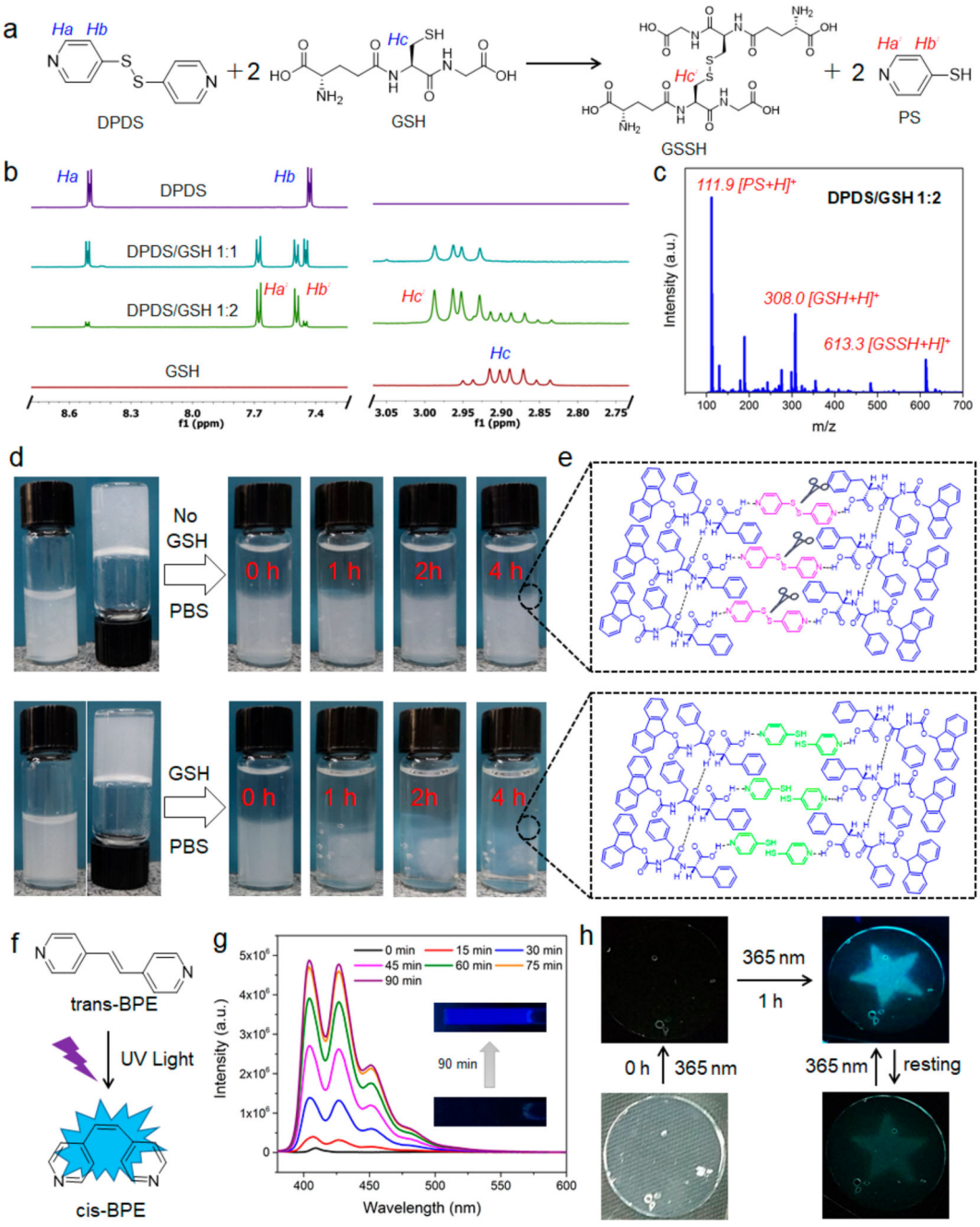

Figure 5.

(a) Proposed chemical reaction of DPDS into PS in the presence of GSH. (b) ^{1}H NMR spectra of DPDS, GSH, and DPDS/GSH mixtures in 1:1 and 1:2 ratios. (c) MS spectrum of 1:2 DPDS/GSH in H_2O. The molar concentration of DPDS is 100 μM. (d) Responsiveness of 1:1 FmocFF/DPDS in the absence and presence of GSH (100 mM) in PBS. (e) Proposed assembly and disassembly of FmocFF/DPDS assembly networks before and after cleavage of disulfide bonds by GSH. (f) Photoinduced enhanced emission of BPE after trans−cis transition. (g) Fluorescence emission traces of BPE (50 μM) in water under UV

irradiation with varying irradiation durations, from 0 to 90 min. Sample was analyzed after the specified irradiation time by a hand-held UV lamp (6 W) at 365 nm. The insets show fluorescent images of BPE sample before and after UV irradiation for 90 min. The excitation wavelength is 365 nm for all the specified fluorescence emissions. (h) Star-shaped fluorescent imprint of the FmocFF/DPDS gel by 1 h UV irradiation and its self-erasing property following rest in visible light.

Europe PMC Funders Author Manuscripts